Eighth International Symposium on Marine Propulsors
smp'24, Berlin, Germany, March 2024

Large eddy simulation of tip vortex interactions for a ducted propulsor*

Thomas Bahati Kroll[1], **Krishnan Mahesh**[2]

[1]Department of Aerospace Engineering & Mechanics, University of Minnesota, Minneapolis, USA
[2]Naval Architecture & Marine Engineering, University of Michigan, Ann Arbor, MI, 48109, USA

ABSTRACT

Experiments by Judge et al. (2001); Chesnakas and Jessup (2003); Oweis et al. (2006a) and Oweis et al. (2006b) studied blade-tip vortex interactions of the ducted marine propeller P5407 at an advance ratio $J = 0.98$ and multiple tip Reynolds numbers. Large-eddy simulation (LES) is used to study these interactions at the same advance ratio and at tip Reynolds number $Re_{tip} = 1.4 \times 10^6$. Two vortex structures termed the tip-leakage vortex (TLV) and trailing-edge vortex (TEV) whose interactions were closely linked to cavitation inception are studied. The TEV is found to be composed of co and counter-rotating small-scale vortices and is not coherent enough to be identified by low-pressure regions. Good agreement is obtained with the experiment for mean loads and flow field. The TLV is revealed to interact with the duct wall boundary layer, inducing upstream, secondary, and counter-rotating vortices. The interaction and merger of these vortices with the TLV form a complex flow field with increased unsteadiness and pressure fluctuations past 50% chord length downstream of the blade tip, supporting the experimental observations of their role in cavitation inception.

Keywords

LES, tip vortex, propeller.

1 INTRODUCTION

Flow structures like the helical tip vortices often characterize the wake of a propulsor operating in design conditions. This is also often where flow phenomena like cavitation occur. For a ducted propulsor, the primary tip vortex has been observed to interact with secondary vortical structures formed at the blade trailing edge with implications on cavitation inception. To study these vortex interactions, propeller P5407 was studied in the experiments by Judge et al. (2001); Chesnakas and Jessup (2003); Oweis et al. (2006a,b) at different propeller tip Reynolds numbers. These experiments identified two vortex structures termed the tip-leakage vortex (TLV) and trailing-edge vortex (TEV) whose interactions link them to cavitation inception. It was hypothesized that inception events occur when the weaker TEV wraps around the stronger TLV before eventually merging further downstream (figure 1). Small-scale vortical structures were observed to undergo strong stretching in this merger process, generating very low instantaneous pressures. Visual and sub-visual cavitation inception is observed up to 50% of the chord length downstream of the propeller trailing-edge tip. However, the mean location of the lowest pressure was located at 10% of the chord length. Altogether, these unsteady interactions were found to be important in understanding the mechanisms that can lead to cavitation inception in ducted propulsors (Oweis et al., 2006b). These experiments had the following additional conclusions.

- The interaction of multi-scale vortices with fine-scale secondary vortices is likely responsible for cavitation inception.
- The presence of small-scale vortices is masked by mean statistics and thus a need to study their unsteady interactions.
- The single-phase fluid flow is a major challenge due to the complex vortex dynamics.

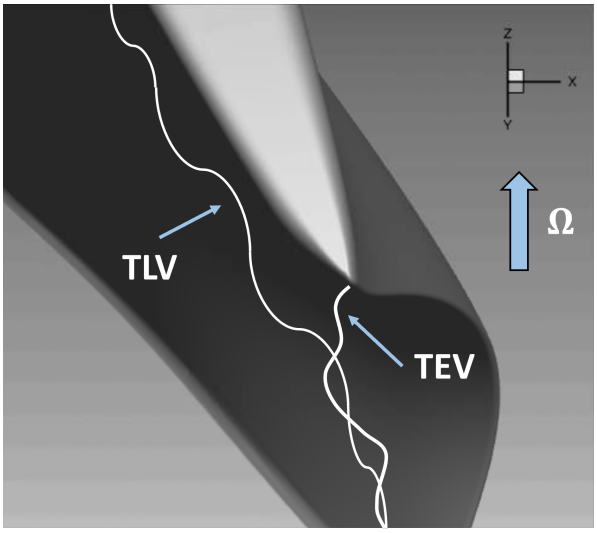

Figure 1: A schematic of the three-bladed propeller P5407 showing the interaction of the tip-leakage vortex (TLV) and trailing-edge vortex (TEV).

*Email for correspondence: krmahesh@umich.edu

This work aims to computationally study single-phase, incompressible flow to gain insights into the vortex dynamics that can lead to high-pressure fluctuations and the increased likelihood of cavitation inception. This flow presents multiple challenges. The high Reynolds number Re requires high-resolution grids in relevant regions of the flow to capture the multi-scale vortex formation and interaction. In addition, the problem requires modeling methods that can capture the evolving unsteady vortex interactions. As Direct Numerical Simulation (DNS) is not feasible, Large Eddy Simulation (LES) is performed using an unstructured overset method. LES resolves a wide range of turbulent lengths and time scales to capture the transient behavior of tip vortex interactions. The use of overset grids provides additional flexibility in the grid generation process and helps maintain good resolution in relevant areas near the propeller blades, duct, and tunnel walls. LES has been used to study similar flow characteristics in turbomachinery flow with insights into the vortex dynamics (You et al., 2004, 2007a,b; Wu et al., 2011a,b, 2012; Miorini et al., 2012).

In the present work, LES using an unstructured overset method is used to study the unsteady vortex interactions for ducted propeller P5407 at tip Reynolds number, $Re_{tip} = 1.4 \times 10^6$ and at an advance ratio of $J = 0.98$. The objectives of this study are to (i) illustrate the ability of LES using an unstructured overset method to predict flow over a ducted propeller in the forward mode of operation, (ii) provide insight into the unsteady tip-region vortex interactions of the TLV and TEV that are crucial to cavitation inception. The paper is organized as follows. The simulation details including the numerical method, geometry, computational grid and boundary conditions are described in section . The results with a comparison to the experiment and insights into the flow field are discussed in section . And finally, the work is summarized in section .

2 SIMULATION DETAILS

2.1 Numerical Method

The incompressible Navier-Stokes equations with an Arbitrary Lagrangian-Eulerian (ALE) formulation are used. The grid velocity is included in the convection term which avoids tracking multiple reference frames for the arbitrary motion of meshes. For LES, large scales are directly accounted for by the spatially filtered Navier-Stokes equations, and small scales are modeled. The filtered Navier-Stokes equations with the ALE formulation are as follows:

$$\begin{aligned} \frac{\partial \overline{u}_i}{\partial t} + \frac{\partial}{\partial x_j}(\overline{u}_i \overline{u}_j - \overline{u}_i V_j) &= -\frac{\partial \overline{p}}{\partial x_i} + \nu \frac{\partial^2 \overline{u}_i}{\partial x_j \partial x_j} - \frac{\partial \tau_{ij}}{\partial x_j}, \\ \frac{\partial \overline{u}_i}{\partial x_i} &= 0, \end{aligned} \tag{1}$$

where u_i is the velocity in the inertial frame, p is the pressure, ν is the kinematic viscosity, V_j is the grid velocity, the overbar $\overline{(.)}$ denotes the spatial filter and $\tau_{ij} = \overline{u_i u_j} - \overline{u}_i \overline{u}_j$ is the sub-grid stress tensor. To model the sub-grid stress terms, the dynamic Smagorinsky model proposed by Germano et al. (1991) and modified by Lilly (1992) is used. In addition, the Lagrangian time scale is dynamically computed based on the surrogate-correlation of the Germano-identity error (Park and Mahesh, 2009). This approach has shown good performance for a variety of flows including a marine propeller in crashback (Verma and Mahesh, 2012).

Mahesh et al. (2004) developed an unstructured numerical algorithm for LES of complex flows that emphasizes discrete kinetic energy conservation, ensuring robustness at high Reynolds numbers without numerical dissipation. This method has been successful in simulating a variety of complex marine flows (Verma et al., 2012; Kumar and Mahesh, 2017; Jang and Mahesh, 2013; Kumar and Mahesh, 2018). The method used in the present computations is an unstructured overset grid method based on the above algorithm of Mahesh et al. (2004) with the capability of solving arbitrary overlapping and moving meshes (see Horne and Mahesh, 2019a,b). It uses an ALE method coupled to a 6 degrees of freedom rigid body equation system (6-DOF) for body motion. At boundary edges of meshes, boundary conditions are obtained by performing flow field reconstructions using overlapping meshes and geometry. This enables the use of body-fitted meshes, ensuring high resolution on the relevant geometries while aiding to save on overall mesh size and increased grid generation flexibility. In addition, this method addresses the conservation challenges of overset methods through use of a volume-conservative supercell interpolation. To address additional computational cost and scaling challenges of overset methods, it uses a novel communication strategy, scaling to $0(10^5)$ meshes and processors. The algorithm has been validated for a variety of problems over a range of Reynolds numbers (Kroll et al., 2020; Kroll and Mahesh, 2022).

2.2 Problem description

The David Taylor 36-inch variable pressure water tunnel (VPWT) was used to perform ducted propeller experiments by Judge et al. (2001); Chesnakas and Jessup (2003); Oweis (2003); Oweis et al. (2006a,b). These experiments were performed at a range of tip Reynolds numbers from $Re_{tip} = 0.7 \times 10^6 - 9.2 \times 10^6$, based on the propeller chord length c with P5407 representing the lower end of this range. The tip Reynolds number is defined as:

$$Re_{tip} = \frac{(U_\infty + \pi D n) * c}{\nu} \tag{2}$$

where U_∞ is the free-stream velocity, D is the propeller disk diameter, n is the rotational speed, ν is the kinematic viscosity and the term $(U_\infty + \pi D n)$ represents the tip speed. In this study, we perform simulations in the lower range of Reynolds numbers at $Re_{tip} = 1.4 \times 10^6$ and advance ratio $J = 0.98$. The advance ratio J characterizes the relative ratio between free-stream velocity and propeller rotation and is defined as:

$$J = \frac{U_\infty}{nD} \tag{3}$$

where U_∞ is the free-stream velocity, D is the propeller disk diameter, $n = \Omega/2\pi$ is the rotational speed where Ω is the rotational velocity.

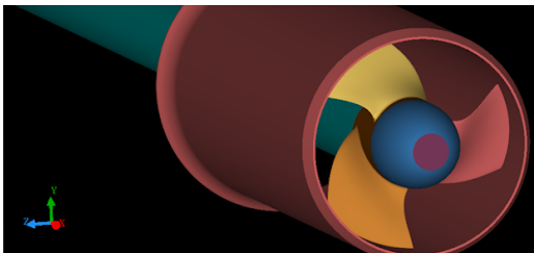

Figure 2: The three-bladed propeller P5407 with a duct attached is visualized. Note that x is the axial direction along the propeller axis. θ is the direction of propeller rotation here being clockwise using the right-hand rule, and r is the radial direction centered at the propeller's central location.

The propeller P5407 has three blades, a constant chord, and a radially varying pitch due to blade twist, skew and rake. It has a blade tip diameter of $D = 12\ inches$ (304.8 mm), an inner duct diameter $D_{di} = 12.188\ inches$ (309.575 mm), an outer duct diameter $D_{do} = 13.215\ inches$ (335.661 mm), a hub diameter $D_h = 4.964\ inches$ (126.086 mm) and a constant chord length of $c = 5.352\ inches$ (135.941 mm). A 12 $inch$ (309.575 mm) diameter bell mouth was installed on the duct inlet, the duct extends $2.000D$ upstream and $0.299D$ downstream of the propeller center. Figure 2 shows the configuration for P5407 which is placed in the open jet section of the 36-inch VPWT with a duct around it. More details on the experimental setup and geometry can be found in Oweis et al. (2006a).

2.3 Boundary conditions, case setup, and geometry

Propeller P5407 has a complex blade geometry due to the radially varying pitch, blade twist, skew, and rake. Mesh generation is essential for a good-quality grid to be used in the LES simulation. The overset methodology adds flexibility to this process as it enables the use of body-fitted, arbitrarily overlapping meshes to provide local control of mesh resolution and quality. In addition, it allows for high grid resolution around the blade without extending this resolution to the far field of the computational domain and significantly increasing the simulation size.

The focus of this study is to provide insights into the blade tip-region vortex interactions. Thus it is important that good quality and resolution is obtained in the tip region. This is accomplished by ensuring the highest resolution achievable in the blade region as well as the blade tip downstream region (θ direction from the blade tip where the tip vortices interact). Therefore, the blade region grid has the highest resolution in the simulation. The resolutions achieved for each local control volume length l ranges $\Delta l^+ = 8 - 30$ in wall units. For the wall-normal blade and duct surface resolution, the local normal direction n achieved is $\Delta n^+ = 3.2$. Because the experiments found that boundary layer tripping on the blade surfaces had no noticeable effects, there is no need to fully resolve the boundary layer on the blades. A copy of this grid is used for each of the three blades in the simulation. Other grids encompass and transition away from the blades. The background grid encompasses the rest of the grids and contains the outer boundaries of the simulation. Overall, there are a total of 9 grids with 8 overset grids. More information on the size and partitioning of the meshes is presented in table 1.

Table 1: Details of the grid for the P5407 LES simulation.

	Grids	CVs ($\times 10^6$)	Procs
Background	1	47.5	1696
Blade	3	16.4	728
Blade Shroud	3	9.6	426
Blade Buffer	1	38.6	1462
Hub/Wake	1	14.4	640
Total	9	178	7260

The background grid configuration resembles that of P5206, where the large rotor is fitted into the 36-inch VPWT and the wake extends into the open jet section of the VPWT. This gives better control of the propeller inflow, crucial to matching the experimental boundary conditions. The inner duct diameter is the same as the P5407 duct. The outer dimension of the domain is $2D$. The domain inflow is $2.0417D$ upstream of the propeller origin or center. The inflow boundary condition is set to the mean flow rate into the duct. This is estimated by integrating profiles from the experiments and normalizing by the free-stream velocity U_∞. These profiles were located at the position $x = -0.3615R$ where R is the propeller radius. A convective boundary condition is set $2D$ downstream of the propeller center in the outlet section. The blade grids are rotated to match the advance ratio $J = 0.98$. The surfaces contained in them are prescribed with $v = \Omega \times R$ boundary conditions, using the rotational velocity $\Omega = 2\pi n$ except for on the duct surface which has no-slip boundary condition. All other surfaces have no-slip boundary conditions. All wall surfaces on the blade, duct, and hub have a minimum wall-normal spacing of $1.667 \times 10^{-4} D$ and a growth ratio of 1.01. The simulations are performed at $Re_{tip} = 1.4 \times 10^6$ with a non-dimensional time step of $\Delta t U_\infty / D = 4.167 \times 10^{-5}$. The final grid configuration can be seen in figure 3.

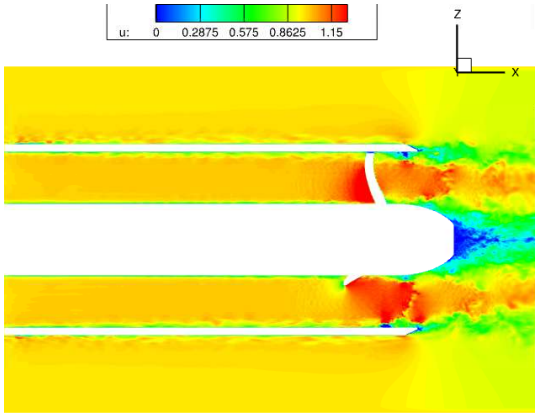

Figure 3: LES simulation showing the contour of instantaneous axial velocity U_x for the propeller P5407. Note the thick boundary layers on the duct surface which were observed in the experiments to be thicker than the tip gap. The flow field quantities are normalized with U_∞.

A total of 10 revolutions or 5 flow domain passes are simulated. The run time for a single revolution was about 23 hours on 7260 processors. The overall computational cost for the 10 revolutions is about 1.6 million CPU hours. Numerical trips are used for the duct boundary layer at $2D$ upstream of the propeller, the location where the duct bellmouth begins. The trip is implemented by applying a steady wall-normal velocity of 0.06% of U_∞. The final selected simulation is run for enough revolutions to ensure flow field and load statistical convergence.

3 RESULTS

3.1 Comparison to experiment

The LES time-averaged flow statistics and load statistics are sampled for 4 revolutions and compared to the experiments of Chesnakas and Jessup (2003); Oweis (2003); Oweis et al. (2006a) and Oweis et al. (2006b). LES flowfield statistics are sampled using sufficient separation times so that there are no correlations in time. This was determined by sampling flow simulation variables at different locations and selecting a time scale that minimized autocorrelation or the measure of the similarity over successive time intervals.

To verify the appropriateness of the mesh resolution, figure 4 shows the influence of the sub-grid-scale (SGS) model near the tip-leakage vortex region at $s = 0$. The simulation eddy-viscosity ν_t normalized by the molecular viscosity ν has a maximum value of about 6. This small magnitude means low utilization of the LES model, suggesting sufficient resolution in the vortex interaction areas.

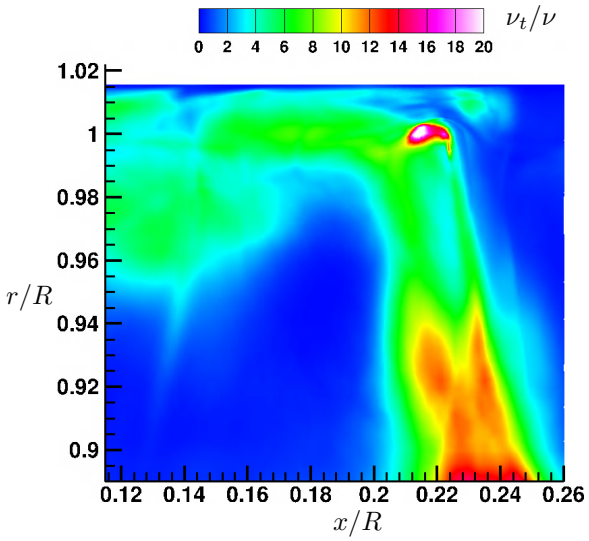

Figure 4: A contour slice showing the eddy-viscosity ν_t normalized by the molecular viscosity ν. This slice is taken in the $x - r$ plane at the propeller trailing-edge tip $s = 0$.

To assess the propeller loads, the propeller thrust T is defined as the axial component of the force. The axial component of the moment of the force is the torque Q. It then follows that the non-dimensional thrust K_T, torque K_Q defined as:

$$K_T = \frac{T}{\rho n^2 D^4}, \qquad K_Q = \frac{Q}{\rho n^2 D^5} \tag{1}$$

where ρ is the fluid density, $\langle K_T \rangle$ represents the mean of the coefficient K_T and $\sigma(K_T)$ the standard deviation.

Table 2: Propeller P5407 ($J = 0.98$): A comparison of load statistics. EXP-1 (Chesnakas and Jessup, 2003), EXP-2 (Oweis, 2003), EXP-3 (Oweis et al., 2006b), LES-P5407 is the current simulation.

	$Re_{tip}(\times 10^6)$	$\langle K_T \rangle$	$\langle K_Q \rangle$
EXP-1	1.4	0.278	0.053
EXP-2	1.4	0.245	0.054
EXP-3	1.4	0.265	0.054
LES-P5407	1.4	0.273	0.054

Table 2 summarizes the load statistics comparison between the LES and various experiments. The LES results show good agreement for the torque coefficient K_Q and K_T is within the scatter of the experiments.

The time-averaged flow statistics from the LES are compared to the three-dimensional LDV experimental data of Chesnakas and Jessup (2003) provided by the Naval Surface Warfare Center, Carderock Division (NSWCCD), (Thad Michael, personal communication). Comparisons are made at various locations along the circumference of the blade in the downstream or θ direction. The arclength is transformed to s coordinates which are centered at the blade trailing-edge tip where:

$$s = \frac{r\theta}{c}, \tag{2}$$

where r is the radial direction, θ is direction of propeller rotation and c is the blade chord. The convention is that $s = 0$ at the propeller trailing-edge tip and it is positive downstream, in the clockwise direction, using the right-hand rule.

Contour slices are taken at the blade tip ($s = 0$) for each of the three blades in the axial and radial plane ($x - r$). Figure 5 shows contour slices of the mean of the θ component of vorticity ω_θ. We see a good overall qualitative agreement. As expected, the vorticity maximum component peaks at the TLV vortex center. It is mostly directed in the positive θ direction (out of the page and clockwise and away from the direction of propeller rotation). The positive θ component is the composition of a majority of the shedding vortices formed at the blade surface, the source of the TLV. A narrow region of vorticity connects the TLV to the blade tip, representing a region dense with the source vortices that are shed off the blade throughout the chord length. We note in the LES contours that upstream, on the duct wall (to the upper left on contours), the TLV induces a secondary, counter-rotating vortex (opposite ω_θ sign).

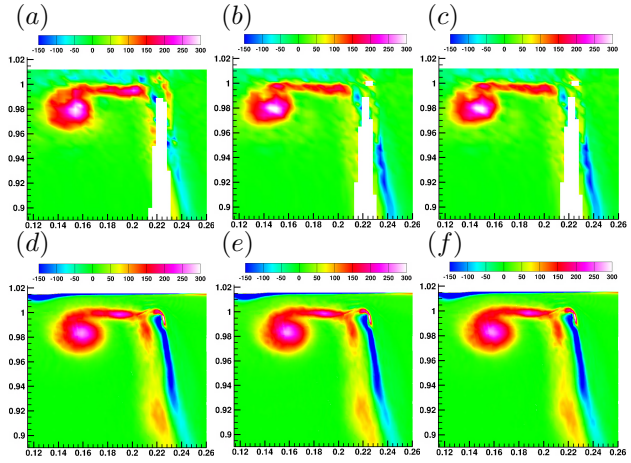

Figure 5: Contours of mean vorticity ω_θ for the 3 individual blades at the blade trailing edge and in the $x-r$ plane where the horizontal axis is x/R and the vertical axis is r/R. (a,b,c) are the LDV from the experiments of Chesnakas and Jessup (2003). (d,e,f) are the current LES. The flow field quantities are normalized with U_∞/R.

More detailed profiles of ω_θ (figure 6) are taken at various locations in the axial direction x/R. Overall we see good agreement, with the peaks within the experimental scatter. Differences near the duct surface are observed as expected due to the lower resolution of the LDV.

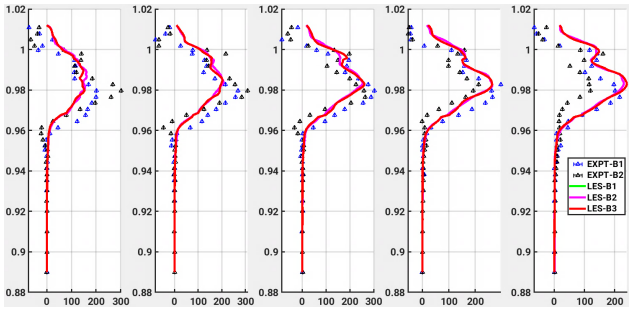

Figure 6: The profiles of the LDV at various axial locations near the TLV center. The vertical axis is r/R while the horizontal axis is mean ω_θ. The experiments of Chesnakas and Jessup (2003) are the symbols while the LES are the solid lines for the different blades. The locations are from left to right $x/R = 0.145$, $x/R = 0.150$, $x/R = 0.154$, $x/R = 0.158$, and $x/R = 0.162$. The flow field quantities are normalized appropriately using U_∞ and R.

Table 3: Propeller P5407 ($J = 0.98$): The mean TLV vortex center locations of the experiment (EXP) of Chesnakas and Jessup (2003) compared to LES in the $x-r$ plane.

	x/R	r/R
EXP Blade 1	0.154	0.979
EXP Blade 2	0.148	0.980
EXP Blade 3	0.157	0.977
LES Blade 1	0.159	0.983
LES Blade 2	0.158	0.983
LES Blade 3	0.159	0.983

The vortex centers, approximated by regions of the highest vorticity are shown in table 3. Overall we see good agreement as the LES individual blade locations are all within 1% of each other, a sign of statistical convergence.

3.2 Multi-scale vortex interactions

In this section, we will show why it is crucial to use a method like LES to capture the unsteady vortex interactions and eventual unsteady pressure drops likely to cause cavitation inception. The TLV is visualized in figure 7(a) using iso-contours of the pressure coefficient C_p defined as:

$$C_p = \frac{p - p_\infty}{\frac{1}{2}\rho U_\infty^2} \tag{3}$$

where p is the local pressure, p_∞ is the reference pressure, U_∞ is the free-stream velocity and ρ is the fluid density. The TLV forms on the blade suction side and is tilted at an angle in the $x-r$ plane. The TEV does not appear to be strong enough or visibly coherent to be visualized with C_p (figure 7a).

Previous experiments showed that instantaneous, multi-scale unsteady vortex interactions play a role in cavitation inception. However, these are not visible with C_p. Figure 7(b,c) uses the $Q-criterion$ vortex identification method to visualize the flow field, revealing a more complex vortex field. Just as in the experiments, the TLV and TEV instantaneous interaction consists of small-scale vortices. Figure 7(c) reveals that these vortices form on the blade surface and feed into the formation of the TLV as a result of the tip leakage flow separating at the blade surface. This is evidenced by the majority of these vortices having a positive ω_θ component throughout the blade chord as they form. It is also important to note that evidence of a coherent TEV is lacking, instead the radial region it is supposed to be located (the blade trailing-edge tip) is composed of and forms a complex mixture of small-scale vortices with positive and negative components of ω_θ shed from the blade tip (figure 7c). The reason why C_p is not a good way to visualize the vortices from the TEV region is that they contain a much higher pressure than the TLV center (figure 7b). Additional interactions arise upstream of the TLV in the axial direction (x), where regions of negative ω_θ represent induced secondary, counter-rotating vortex structures formed by the interaction of the TLV and the boundary layer on the duct wall.

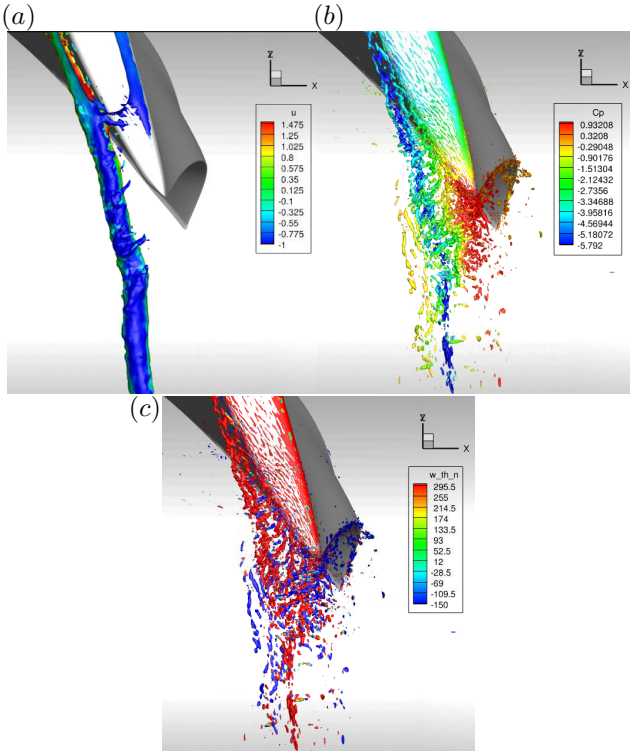

Figure 7: (a) Instantaneous iso-contours of the pressure coefficient $C_p = -3.5$ coloured by the axial velocity U_x. Instantaneous iso-contours of $Q - criterion = 57600s^{-2}$ (b) coloured by the pressure coefficient C_p and (c) coloured by the ω_θ. The flow field quantities are normalized appropriately using ρ, U_∞ and R.

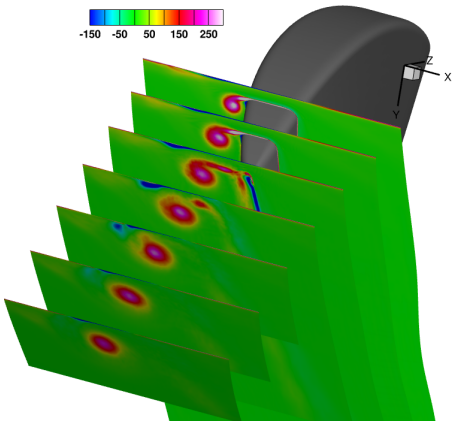

Figure 8: The θ component of mean vorticity ω_θ along slices of s. The slices step $s = 0.083$ with the propeller trailing edge at $s = 0$. The flow field quantities are normalized with U_∞/R.

To further confirm the prior observations on the instantaneous flow field, contours of mean ω_θ are taken along slices of s in figure 8. The TEV composition is confirmed, as the high vorticity region originating from the blade trailing edge is evidence of the small-scale vortices of varying components of vorticity with a majority in the positive θ direction. It appears these vortices and their interaction are not strong enough to form a coherent vortex like the TLV. These vortices are then observed to feed into and merge with the TLV, further downstream. The upstream negative ω_θ region in figure 8 confirms the presence of upstream, secondary, induced counter-rotating vortices formed by the duct wall boundary layer and TLV interaction. Overall, these observations confirm that these essential small-scale vortices can be masked by mean statistics and to study their interactions requires capturing them in an unsteady manner.

3.3 The vortex merger process

The experiments revealed a merger of the trailing-edge vortex (TEV) and the stronger tip-leakage vortex (TLV). In the instantaneous flow field (figure 7), this is not obvious. However, the flow-field mean statistics provide insights into this merger process.

The high positive mean ω_θ region of the TEV in figure 8 reveals that instantaneously, the small-scale vortical structures of the TEV approach and begin to merge with the TLV at around $s = 0.10$. The lowest mean pressure observed in the computation is approximately at $s = 0.15$. Around this location, the TEV small-scale vortices appear to physically begin merging with the TLV, revealing the influence of these vortices. The mean vorticity region of the TLV is still irregularly shaped as these vortices continue their merge at $s = 0.30$ (figure 8) suggesting the interaction of the small-scale vortices of the TEV and TLV is still occurring. This hints to why high-pressure fluctuations leading to cavitation are observed experimentally even further downstream at $s = 0.5$ as this merger process that deforms and stretches the small-scale vortices continues much further than where it begins as these vortices continue to orbit the TLV. PIV from (Chesnakas and Jessup, 2003; Oweis, 2003; Oweis et al., 2006a,b) also observes these distinct small-scale vortices from the TEV orbiting and then merging with the TLV as s increases away from the blade tip. This complex process continues even further downstream leading to increased unsteadiness of the flow field. The interaction of the TLV and TEV leads to finer and smaller vortex filaments getting stretched and distorted possibly leading to transient pressure drops and possible cavitation inception. It was not distinguishable whether these small-scale vortices were ones mostly originated from the TEV or ones formed during the merger process.

Additional interactions not previously observed in the experiments are shown in figure 9 with the mean vorticity magnitude ω_{mag}, mean square pressure fluctuations $\overline{p'p'}$, and the resolved turbulent kinetic energy k at various slices of s. In the previous section, induced secondary, counter-rotating vortex structures were observed in the upstream, axial direction (x). We observe that these also interact with the TLV at around $s = 0.2-0.4$. Figure 9 shows that as the induced vortex breaks down, the small-scale vortices also start merging with the TLV further increasing unsteadiness downstream in s. This interaction further complicates the already complex flow field since in addition to the TEV, this induced vortex feeds counter-rotating small-scale vortices to the TLV. This means that there is a possibility that

these also contribute to the pressure fluctuations and possible cavitation inception further downstream in s as observed in the experiments.

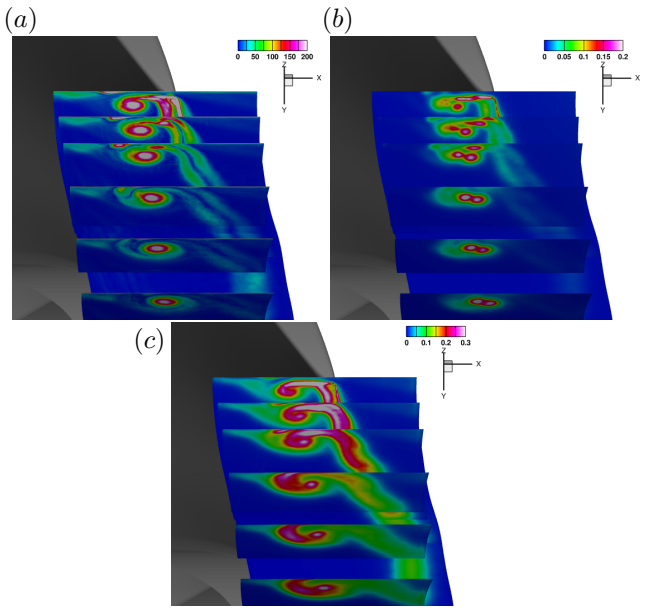

Figure 9: Contours along slices of s. The magnitude of mean vorticity ω_{mag} is (a) the mean square pressure fluctuations $\overline{p'p'}$ is (b) and resolved turbulent kinetic energy k is (c). The slices start from the propeller blade trailing edge at $s = 0.0$, $s = 0.056$, $s = 0.112$, $s = 0.2$, $s = 0.3$ and $s = 0.4$. The flow field quantities are normalized appropriately using ρ, U_∞ and R.

4 SUMMARY

An unstructured overset method with LES to study the ducted propeller P5407 at tip Reynolds number $Re_{tip} = 1.4 \times 10^6$. The overset method enables the creation of simple grids with a good resolution that represents well the complex geometries of the rotor blades, and duct. Validation is performed with the propeller load statistics showing good agreement. The flow field statistics contours and profiles are also compared to experimental LDV, showing good agreement.

The instantaneous pressure field reveals a strong TLV as observed in the experiments. A complex mixture of small-scale vortices visible through other vortex visualization methods like the $Q - criterion$ is confirmed. The TEV is not strong enough to be visualized using the pressure coefficient C_p and is composed of a complex mixture of co and counter-rotating small-scale vortices. Most of these vortices have vorticity in the positive θ direction just like the TLV and as they interact with the TLV, they begin to merge at the lowest mean pressure location around 15% of the chord length downstream of the blade tip, continuing even further past 30% of the chord length. A new merger process is observed for the first time where the TLV-induced upstream, secondary counter-rotating vortices merge with the TLV at around $20\% - 40\%$ of the chord length downstream of the blade tip. This further complicates the overall interaction which now consists of co and counter-rotating small-scale vortices from the TEV as well as mostly counter-rotating small-scale vortices from this induced vortex. The complex and unsteady interactions of the TLV with both the TEV and the secondary-induced vortex could explain the experimental observation of sub-visual cavitation at around 50% chord length downstream of the blade tip.

Future work aims to simulate a finer grid of the present case to ensure grid convergence with a similar comparison to experiments. Further analysis of the instantaneous pressure fluctuations and temporal correlation to the observed small-scale vortices can lead to further insight into the source and locations of cavitation inception.

ACKNOWLEDGMENTS

This work was supported by the United States Office of Naval Research (ONR) under ONR Grant N00014-21-1-2455 with Dr. Yin-Lu Young as grant monitor. Computational resources were provided by the U.S. Army Engineer Research and Development Center (ERDC) in Vicksburg, Mississippi on the Cray XC40/50, Onyx of High Performance Computing Modernization Program (HPCMP) and the Minnesota Supercomputing Institute (MSI) at the University of Minnesota.

REFERENCES

Chesnakas, Christopher J and Jessup, Stuart D. "Tip-vortex induced cavitation on a ducted propulsor". In Fluids Engineering Division Summer Meeting, volume 36967, pages 257–267, 2003.

Germano, M., Piomelli, U., Moin, P., and Cabot, W. H. "A dynamic subgrid–scale eddy viscosity model". Physics of Fluids A, 3:7:1760, 1991.

Horne, Wyatt James and Mahesh, Krishnan. "A massively-parallel, unstructured overset method for mesh connectivity". Journal of Computational Physics, 376:585–596, 2019a.

Horne, Wyatt James and Mahesh, Krishnan. "A massively-parallel, unstructured overset method to simulate moving bodies in turbulent flows". Journal of Computational Physics, 397:108790, 2019b.

Jang, H. and Mahesh, K. "Large eddy simulation of flow around a reverse rotating propeller". Journal of Fluid Mechanics, 729:151–179, 2013.

Judge, Carolyn Q, Oweis, Ghanem F, Ceccio, Steven L, Jessup, Stuart D, Chesnakas, Christopher J, and Fry, David J. "Tip-leakage vortex inception on a ducted rotor". http://resolver. caltech. edu/cav2001: sessionA6. 001, 2001.

Kroll, T., Morse, N., Horne, W., and Mahesh, K. "Large eddy simulation of marine flows over complex geometries using a massively parallel unstructured overset method". In Proceedings of the 33rd Symposium on Naval Hydrodynamics, Osaka, Japan, 2020.

Kroll, T. B. and Mahesh, K. "Large-eddy simulation of a ducted propeller in crashback". Flow, 2:E–4, 2022. doi: 10.1017/flo.2021.18.

Kumar, P. and Mahesh, K. "Large eddy simulation of propeller wake instabilities". Journal of Fluid Mechanics, 814:361–396, 2017.

Kumar, P. and Mahesh, K. "Large-eddy simulation of flow over an axisymmetric body of revolution". Journal of Fluid Mechanics, 853:537–563, 2018.

Lilly, D. K. "A proposed modification of the Germano subgrid–scale closure model". Physics of Fluids A, 4:3: 633, 1992.

Mahesh, K., Constantinescu, G., and Moin, P. "A numerical method for large–eddy simulation in complex geometries". Journal of Computational Physics, 197:1: 215, 2004.

Miorini, Rinaldo L, Wu, Huixuan, and Katz, Joseph. "The internal structure of the tip leakage vortex within the rotor of an axial waterjet pump". Journal of Turbomachinery, 50(11):2574–2587, 2012.

Oweis, G. F. An Experimental Investigation into the Dynamics of Propeller Tip Vortices and the Associated Cavitation Noise. PhD thesis, University of Michigan, USA, 2003.

Oweis, G. F., Fry, D., Chesnakas, C., Jessup, S., and Ceccio, S. L. "Development of a tip-leakage flow. part 1: The flow over a range of reynolds numbers.". Journal of Fluids Engineering, 128:751–764, 2006a.

Oweis, G. F., Fry, D., Chesnakas, C., Jessup, S., and Ceccio, S. L. "Tip-leakage flow. part 2: Comparison between the ducted aand un-ducted rotor.". Journal of Fluids Engineering, 128:765–773, 2006b.

Park, N. and Mahesh, K. "Reduction of the Germano-identity error in the dynamic Smagorinsky model". Physics of Fluids (1994-present), 21(6):065106, 2009.

Verma, A. and Mahesh, K. "A Lagrangian subgrid-scale model with dynamic estimation of Lagrangian time scale for large eddy simulation of complex flows". Physics of Fluids (1994-present), 24(8):085101, 2012.

Verma, A., Jang, H., and Mahesh, K. "The effect of an upstream hull on a propeller in reverse rotation". Journal of Fluid Mechanics, 704:61–88, 2012.

Wu, Huixuan, Miorini, Rinaldo L, and Katz, Joseph. "Measurements of the tip leakage vortex structures and turbulence in the meridional plane of an axial water-jet pump". Experiments in Fluids, 50(4):989–1003, 2011a.

Wu, Huixuan, Tan, David, Miorini, Rinaldo L, and Katz, Joseph. "Three-dimensional flow structures and associated turbulence in the tip region of a waterjet pump rotor blade". Experiments in fluids, 51(6):1721–1737, 2011b.

Wu, Huixuan, Miorini, Rinaldo L, Tan, David, and Katz, Joseph. "Turbulence within the tip-leakage vortex of an axial waterjet pump". AIAA journal, 134, 2012.

You, Donghyun, Mittal, Rajat, Wang, Meng, and Moin, Parviz. "Computational methodology for large-eddy simulation of tip-clearance flows". AIAA journal, 42 (2):271–279, 2004.

You, Donghyun, Wang, Meng, Moin, Parviz, and Mittal, Rajat. "Large-eddy simulation analysis of mechanisms for viscous losses in a turbomachinery tip-clearance flow". Journal of Fluid Mechanics, 586:177–204, 2007a.

You, Donghyun, Wang, Meng, Moin, Parviz, and Mittal, Rajat. "Vortex dynamics and low-pressure fluctuations in the tip-clearance flow". Journal of Fluids Engineering, 129:1002–1014, 2007b.